

Tailoring the structure and acid site accessibility of mordenite zeolite for hydroisomerisation of *n*-hexane

Jana Pastvova^{a,b}, Radim Pilar^a, Jaroslava Moravkova^a, Dalibor Kaucky^a, Jiri Rathousky^a, Stepan Sklenak^a, Petr Sazama^{a,*}

^a J. Heyrovsky Institute of Physical Chemistry, Academy of Sciences of the Czech Republic, Dolejskova 3, 182 23 Prague, Czech Republic

^b University of Pardubice, Studentska 95, Pardubice, 532 10, Czech Republic

ARTICLE INFO

Keywords:

Isomerisation
n-hexane
Mordenite (MOR) zeolites
Supermicroporosity
Micromesoporous structure

ABSTRACT

Mordenite zeolites with diffusion-restricted access to the acid sites located in mono-dimensional 12-ring channels and 8-ring side pockets have found broad applications as catalysts for hydroisomerisation of linear C₅ and C₆ alkanes and other highly relevant acid-catalysed processes. The accessibility of the porous structure of mordenite (MOR) zeolite is traditionally enhanced by dealumination, but this is invariably connected with a dramatic reduction in the aluminium content and corresponding concentration of the acid sites in the zeolites. Here we describe the preparation of MOR zeolite with high micropore volume, three-dimensional supermicropores ($d \sim 7.5$ Å) and good acid site accessibility by concurrent extraction of Si and Al using postsynthesis fluorination-alkaline-acid treatment. The concurrent extraction of Si and Al enables formation of more developed supermicroporous structure and preservation of the molecular Si/Al. The procedure yields MOR with a crystalline structure in which the Si/Al ratio and the micropore volume can be tailored (Si/Al from ~ 6 , V_{MI} up to 0.25 cm³·g⁻¹) by the chemical conditions of the treatment. The Al-rich 3D supermicroporous structure with accessible Brønsted and Lewis active sites provides strongly enhanced activity, selectivity and long-term catalytic stability in the transformation of *n*-hexane into the corresponding branched isomers.

1. Introduction

The catalytic hydroisomerisation of linear C₅ and C₆ alkanes as an integral part of the production of automotive gasoline has become a process performed on an impressively large scale. While the chlorinated catalysts in the other large-scale catalytic acid-catalysed processes have been displaced by catalysts based mainly on zeolites, environmentally problematic chlorinated catalysts are still predominantly used in the hydroisomerisation process for their superior activity exceeding that of zeolite catalysts [1,2]. The high activity of chlorinated catalysts allows performance of the hydroisomerisation process at low temperatures (about 150 °C), where the thermodynamic equilibrium is inclined towards the desired multi-branched isomers with high octane number [2]. In contrast, the relatively low zeolite activity means that the reaction must be performed at much higher temperatures (250–300 °C) where, for thermodynamic reasons, the proportion of the two-branched and mono-branched isomers is insufficiently low for modern high-octane automotive fuels [2]. Although besides problematic chlorinated alumina based catalysts, some perspective alternatives were in parallel developed, these still suffer considerable disadvantages. Tungstated

zirconia could show enhanced low-temperature-activity but still suffer from unsolved deactivation/regeneration, which hinder their large-scale application [3]. Strongly acidic sulphated zirconia provides a lower reaction rate compared to chlorinated alumina [4,5]. Previous studies have shown that the activity of zeolites in *n*-hexane hydroisomerisation is controlled by interplay of the concentration of the acidic centres and accessibility of the acid sites for the *n*-hexane molecule in the micropore reaction space, allowing effective formation of the transition state [6–8]. The high concentration and proximity of Brønsted sites facilitate synergistic effects that substantially shift the conversion to the lower temperature range important for the formation of di-branched isomers with a high octane number [9].

Zeolites with mordenite structure are among the most active and selective zeolite catalysts reported in the literature and are used in industrial catalytic processes [6,10–14]. A high concentration of acidic centres in a zeolite with mordenite structure is readily available due to the synthesis of mordenite zeolites with high Al content in the structural framework (Si/Al ~ 5) [15]. However, the accessibility of the acid sites in the channel system of the mordenite zeolite comprising mono-dimensional straight channels with twelve-membered ring (12-ring)

* Corresponding author.

E-mail address: petr.sazama@jh-inst.cas.cz (P. Sazama).

openings and side pockets with 8-ring openings is diffusion-restricted [7,9–11,14]. The small size of the opening of the side pockets ($2.6 \text{ \AA} \times 5.7 \text{ \AA}$) and the kinetic diameters of linear (4.3 \AA), mono-branched (5.0 \AA – 5.6 \AA) and di-branched (5.8 \AA – 6.2 \AA) hexane isomers limit the accessibility of the acidic centres in the side pocket [9,11,15–17]. The openings of the main channel ($6.5 \text{ \AA} \times 7.0 \text{ \AA}$) allow for easy interaction of all the hexane isomers with acid sites located in the main channel; however, the monodimensional channel limits molecular transport and the long residence time reduces the selectivity of the reaction due to side cracking reactions that lead to the formation of undesired C_1 – C_4 molecules [9]. An increase in the accessibility of acidic centres in MOR catalysts can be easily achieved by partial dealumination. The hydrolysis of the Al–O–Si bond and the extraction of the Al atom from the framework during dealumination yield large deformed elongated rings or merging of the two 8-rings, providing a large void space depending on the T site of the extracted atom [9]. The formation of these secondary micropores enables the diffusion of large molecules to the active sites [18]. However, the decrease in the concentration of aluminium in the framework is associated with a significant decrease in the concentration of acidic Brønsted sites limiting the activity of the resulting catalyst.

In the present study, we attempted to create mordenite zeolites with enhanced activity for hydroisomerisation of *n*-hexane that contain a high concentration of aluminium and corresponding concentration of acid sites readily accessible for the hexane molecules. For this purpose, we modified the structure of mordenite zeolite with a high content of lattice aluminium (Si/Al 5.8) by postsynthesis concurrent extraction of Si and Al atoms from the framework using fluorination-alkaline-acid treatments. This modification provides an increase in the dimensions of the channel openings, enlargement of the micropores, 3D interconnection of the micropores as well as the formation of acidic sites with enhanced activity. The combination of the super-mesoporosity and the occurrence of highly active acidic sites dramatically increase the activity of mordenite zeolites in the hydroisomerisation of *n*-hexane to its branched isomers. The high activity shifts the window of operating temperatures to the thermodynamically more suitable area for the formation of di-branched isomers.

2. Experimental

2.1. Preparation of MOR zeolites

Mordenite zeolite (Zeolyst Int., CBV 10 A molar Si/Al 5.8), denoted as MOR/5.8, was used for preparation of mordenites with enhanced accessibility of micropores using postsynthesis fluorination-alkaline-acid leaching procedures (Fig. 1). MOR/5.8 was treated by fluorination-alkaline leaching with various concentrations of NH_4F and NaOH and subsequently by mild dealumination. Typically, 5 g of MOR zeolite was impregnated with 15 ml aqueous solutions of NH_4F at room temperature, kept at RT for 8 h and was then dried at 120°C for 12 h and calcined at 550°C for 3 h. The alkaline treatments were applied to the fluorinated zeolites (1 g of fluorinated MOR per 30 ml NaOH solution stirred in a beaker at a temperature of 85°C for 30 min). Prepared catalysts are denoted as MOR-XF/Y, where X is the concentration of NH_4F and Y is the molar ratio of Si/Al. In the 1st series, concentrations of 0.36 M NH_4F and 0.2 M NaOH solutions were used and the sample was denoted as MOR-0.36 F/5.7. The 2_{nd} series was prepared using 0.5 M NH_4F and 0.4 M NaOH solutions and the sample denoted as MOR-0.5 F/5.6. 1 M NH_4F and 0.4 M NaOH solutions were used for preparation of the 3rd series and the sample was denoted as MOR-F/5.4. The 4th series was prepared using 4 M NH_4F and 0.4 M NaOH solutions and the sample was designated as MOR-4 F/6.2. Finally, after fluorination and alkaline treatment, the samples were mildly dealuminated by adding 30 ml of 0.1 M HNO_3 per 1 g prepared MOR at 50°C for 15 min and were designated as deAl-MOR-0.36 F/7.0, deAl-MOR-0.5 F/6.5, deAl-MOR-1 F/6.8 and deAl-MOR-4 F/6.9, respectively. For the 5th

series, the parent MOR zeolite was treated only by dealumination with HNO_3 (1 g parent MOR zeolite was added to 30 ml 0.1 M HNO_3 at 50°C for 15 min) and the sample was denoted as deAl-MOR/6.6. 100 ml 0.5 M NH_4NO_3 was employed per 1 g zeolite at RT (three times over 12 h) to obtain the ammonium form of the zeolites. To obtain the hydroisomerisation catalysts, Pt was introduced into the NH_4 -form of the MOR zeolites. Pre-dried (at 105°C for 2 h) powder samples were impregnated with an H_2PtCl_6 solution to yield 1.5 wt. % of Pt. The amount of distilled water used for preparation of the impregnation solutions corresponded to the porous volume of each zeolite and was typically in the range $0.5 - 1.0 \text{ cm}^3 \cdot \text{g}^{-1}$.

2.2. Structural and textural analysis

The diffraction patterns of the zeolites were collected on the Bruker AXSD8 Advance diffractometer (Bruker, U.S.A.) with Cu $K\alpha$ radiation with a graphite monochromator and a position sensitive detector (Vântec-1) in Bragg–Brentano geometry. The chemical compositions of the parent and prepared Pt-zeolites were determined by X-ray fluorescence spectroscopy using a Performix XRF-spectrometer (Thermo ARL, Switzerland). The samples were measured and evaluated using UNIQ-UANT5 software. The texture parameters of modified zeolitic materials were determined from the analysis of the N_2 adsorption isotherms at the boiling point of liquid nitrogen (77 K) using the Micromeritics ASAP 2010 apparatus and of the Ar adsorption isotherms at the boiling point of liquid nitrogen (77 K) using the Micromeritics 3Flex system. Prior to the adsorption measurements, the samples were outgassed at 240°C for 24 h. The micropore volume was determined by the Broekhoff-de Boer t-plot method. In this method, the isotherm of nitrogen at 77 K for the studied sample is compared with a suitable standard isotherm, which is explicitly expressed by a thickness equation as representative of layer thicknesses on comparable type of material. In the derivation of the thickness equation, Broekhoff and de Boer related the thickness of the adsorbed film to the total chemical potential of the adsorbed layer rather than assuming thickness to be solely dependent on relative pressure [19]. The total pore volume (V_{tot}) was obtained from the adsorption at a relative pressure of 0.8 converted to the corresponding volume of liquid nitrogen. A relative pressure of 0.8 should ensure the complete filling of the pores by N_2 and, at the same time, this pressure is low enough to avoid substantial condensation of nitrogen in the interstitial space between zeolite particles. The mesopore size distribution was calculated using DFT method based on a model for the adsorption of nitrogen on oxidic surfaces. The Ar adsorption isotherms at the boiling point of liquid nitrogen were employed for the analysis of the micropore size distribution, as the spherical molecule of Ar is more suitable for analysis of sub-nanometer microporous texture than diatomic molecules of nitrogen with a quadrupole moment. Micropore size distribution was calculated by the Horwath-Kawazoe method used in the Saito-Foley extension to cylindrical pores applicable to zeolite studies. The Cheng-Yang correction for the non-ideality of the two-dimensional behaviour of the adsorbed gas was taken into account. In the Horwath-Kawazoe expansion of the model of Everett and Powl describing the potential energy of a single adsorbate molecule confined in a pore, the space in the pore is assumed to be filled with adsorbate molecules [19]. In the case of a filled pore adsorbate-adsorbate-adsorbent interaction contributes a potential in addition to the adsorbate-adsorbent interaction. By averaging the potential over the space within the pore an expression for average interaction energy is obtained, which provides the relationship between the relative equilibrium pressure of the adsorbate and the pore width. Later on, Saito and Foley extended the Horwath-Kawazoe approach by using a cylindrical potential to obtain a method better applicable to studies of zeolites. Finally Cheng and Yang corrected the non-linearity of the adsorbed gas which was not included in the original Horwath-Kawazoe equation [19]. All the methods used were performed using Micromeritics software. As the adsorption experiment using argon were carried out at a temperature of the boiling

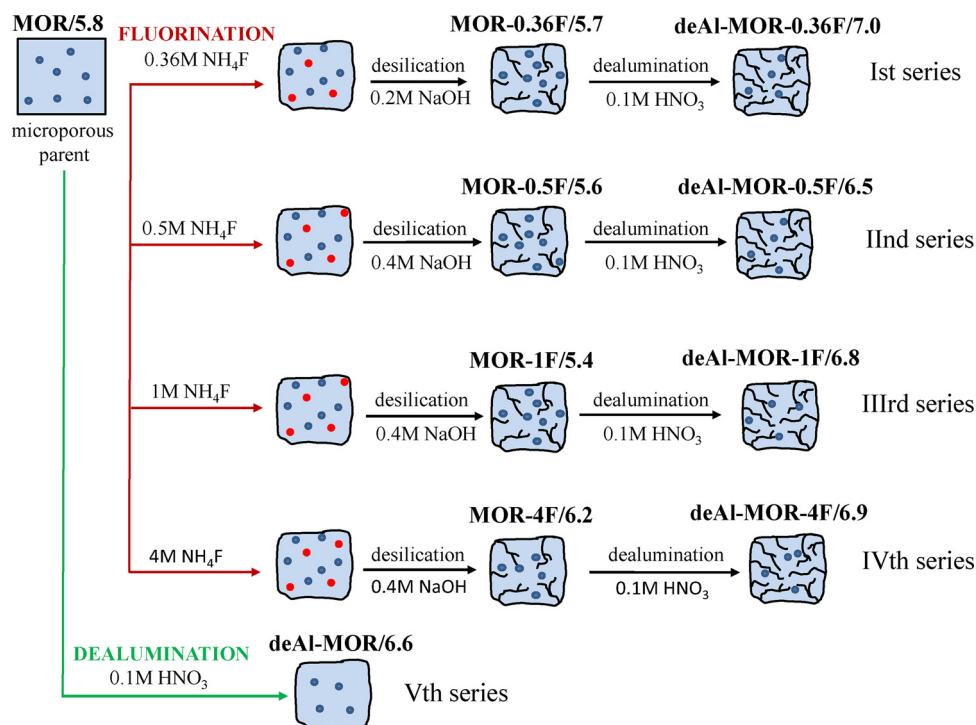


Fig. 1. Scheme of the preparation of the supermicroporous mordenites using postsynthesis fluorination-alkaline-acid (Series I-IV), and acid (Series V) treatments.

point of liquid nitrogen, about 10 K below the boiling point of liquid argon, the total pore volume determined from the argon isotherms was corrected. According to the Gurvitsch rule, the volume of liquid condensed in the pores of a porous solid from a condensable gas near its saturation vapour pressure is equivalent to the volume of the pores and should be practically the same for different adsorptives [19]. Therefore, the adsorption isotherms of argon were normalised by multiplying the Ar adsorption by the ratio of total pore volumes $V_{\text{tot N}_2}/V_{\text{tot Ar}}$. The mesoporous volume V_{ME} and surface area were also calculated from the Ar adsorption isotherms. A Hitachi S-4800 scanning electron microscope (Hitachi, Japan) was used to obtain the SEM images. The HR-TEM micrographs were obtained on a JEM 3010 microscope (JEOL, Japan) equipped with a LaB₆ cathode, operated at 300 kV. Before analysis, MOR zeolite samples were calcined at 500 °C in the air and subsequently reduced in a stream of H₂ at 250 °C. The FTIR spectra of the H-forms of the zeolites were measured on a Nicolet nexus 670 FTIR (Thermo Nicolet Co., U.S.A.). Self-supporting wafers were made from the MOR zeolite samples and inserted into the metal holder in the IR cell. The wafers of zeolite samples were evacuated at 450 °C maintained for 3 h and then recorded at RT by collecting 256 scans at 2 cm⁻¹ resolution for each spectrum. CD₃CN was used as a molecular probe for analysis of the concentration of Brønsted and Lewis acid sites. CD₃CN was adsorbed at a partial pressure of 10 Torr for 20 min at RT and subsequently desorbed for 15 min at RT. The resulting IR spectra of the stretching C≡N vibrations and the extinction coefficients $\epsilon_B = 2.05 \text{ cm} \cdot \mu\text{mol}^{-1}$ and $\epsilon_L = 3.60 \text{ cm} \cdot \mu\text{mol}^{-1}$ were used for calculations of the acidic Brønsted and Lewis site concentrations [16]. The accessibility of the OH groups for *n*-hexane in the MOR zeolites was measured using the adsorption of *n*-hexane. The *n*-hexane was adsorbed on the dehydrated samples at a vapour pressure of 1.4 Torr for 20 min at RT with gradual desorption to 0.005 Torr at RT. The accessibility of the OH groups in the MOR zeolite samples was determined by subtracting the intensity of the absorption bands of the stretching vibration mode of the OH in the spectra of dehydrated MOR before and after adsorption of *n*-hexane. Details of the method are described elsewhere [8]. Information on the oxidation and coordination states of Pt particles in the zeolite was obtained using the method of CO adsorption as a

molecular probe in FTIR spectroscopy. Before adsorption of CO, the zeolite samples were heated at 450 °C for 1 h and then activated by reduction in H₂. Hydrogenation of the zeolite samples was performed by gradually heating the sample from RT to 250 °C, which was maintained for 1 h. Subsequently, the samples of Pt/H-MOR zeolite were evacuated and CO was introduced for 30 min. Finally, the IR cell with the samples was degassed and the spectra were recorded at RT. The solid state ²⁷Al MAS NMR method was used for characterisation of the Al species with different coordination in the zeolite. The experiments were performed on a Bruker Avance 500 MHz Wide-Bore spectrometer (Bruker, U.S.A.) equipped with a 4 mm double-resonance MAS NMR probe head. The ²⁷Al MAS NMR spectra of the fully hydrated samples were measured with a high-power decoupling pulse sequence with a p/12 (0.7 μs) excitation pulse, 1 s relaxation delay and rotation speed of 12 kHz. The chemical shifts were referred to an aqueous solution of Al(NO₃)₃.

2.3. Hydroisomerisation of *n*-hexane

The catalytic activity in hydroisomerisation of *n*-hexane to the corresponding iso-C₆ isomers was measured in a U-shaped glass through-flow reactor with catalyst loading of 0.5 g on a porous glass septum. The reactants were preheated in spiral tubing in the inlet part of the reactor. Before each catalytic experiment, activation of the Pt/MOR-zeolite was carried out in an oxygen stream at 450 °C for 3 h and then the zeolite was cleaned with pure nitrogen for 15 min. After calcination, the temperature was lowered to 250 °C and the catalyst was reduced in a mixture of 80 mol % H₂ + 20 mol % N₂ at 250 °C for 1 h. Then 1 mol % of *n*-hexane was fed into this mixture using a glass saturator kept at the selected temperature. The total gas flow was set at 66 cm³·min⁻¹, corresponding to GHSV 5 000 and WSHV 0.25 h⁻¹. The reactor temperature was kept in the desired range of 125–325 °C, controlled by an inserted K-thermocouple. The reaction products containing *n*-C₆, iso-C₆ and low molecular products (i.e.: C₁, C₂, C₃, C₄ and iso-C₄, C₅ and iso-C₅) were analysed by an on-line connected GC (Finnigan 9001), equipped with a capillary column (type: Al₂O₃/KCl, dimensions: length × inner diameter × inner layer:

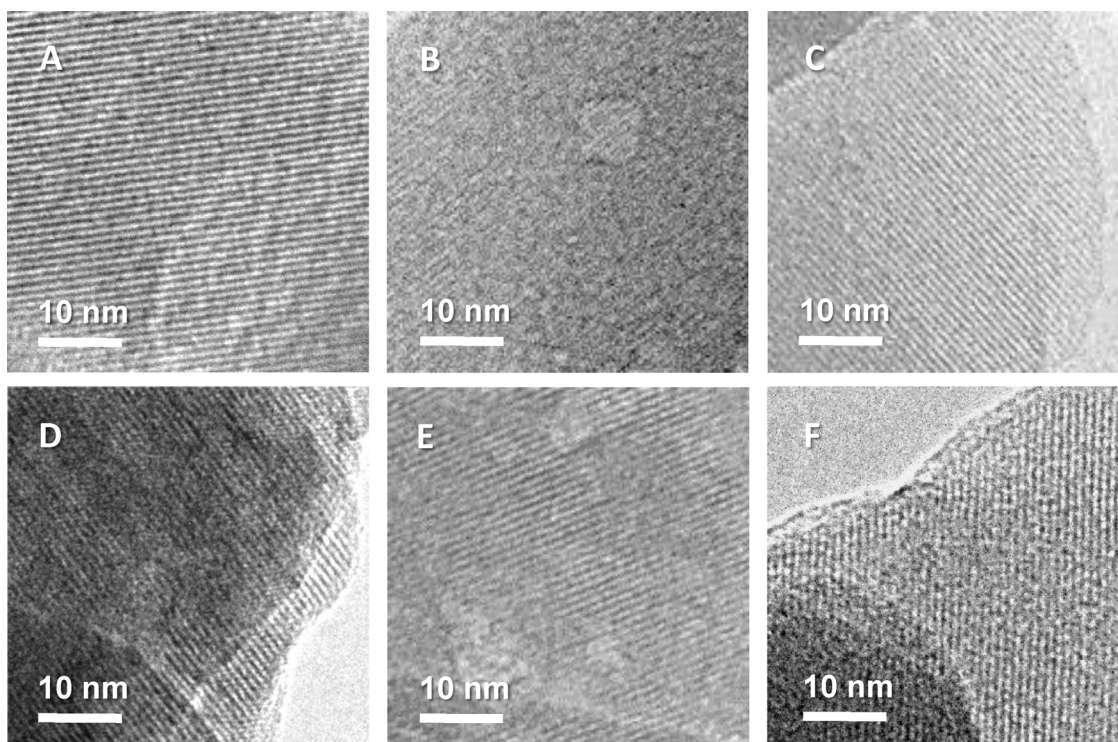


Fig. 2. Representative HR-TEM images of A) parent MOR/5.8 mordenite, B) MOR-0.36 F/5.8, C) deAl-MOR-0.36 F/7.0, D) MOR-1 F/5.4, E) deAl-MOR-1 F/6.8, and F) deAl-MOR/6.6.

50m × 0.32 mm × 5 μm) and conventional FID detector. He 5.0 purity as carrier gas for the column (with input pressure 4.2 atm and flow rate 1.2 cm³.min⁻¹ STP) was used. The following temperature program was used: Temperature range 40–100 °C with the heating rate 2.5 °C.min⁻¹, then 100–180 °C with rate 5 °C.min⁻¹, and 180–200 °C with rate 7.5 °C.min⁻¹. A steady-state regime was typically attained during approx. 0.5–1 h of time-on-stream.

3. Results and discussion

3.1. Structural analysis

3.1.1. Formation of supermicroporous structure in mordenite zeolites

The well-developed crystalline structure of parent MOR/5.8 is manifested by smooth lattice fringes in a representative HR-TEM image (Fig. 2A), high intensities of the characteristic lines in the X-ray diffractogram without impurity phases (Fig. 3), a micropore volume of 0.16 cm³.g⁻¹ (Table 1) and size distribution of the micropores corresponding to the mordenite structure (Fig. 4). Fluorination-alkaline treatment (Fig. 5) resulted in a slight decrease in the intensity of the diffraction lines associated with reducing the density of the structural framework and slight roughness of the lattice fringes of the crystalline structure in the HR-TEM images. Use of fluorination-alkaline treatment with concentrations of 0.36 M NH₄F in the 1st and 0.5 M NH₄F in the 2nd series resulted in an increase in the micropore volume to about 0.2 cm³/g, with a further increase after mild dealumination to 0.23 and 0.24 cm³/g, respectively, with only minor creation of mesopores with a volume of 0.05 and 0.06 cm³/g, respectively, also visible at the HR-TEM images. In the first series, the micropore volume is increased mainly by an increase in the number of micropores with dimensions of about 0.7 nm. This enhancement could be ascribed to enlargement of the narrow openings of the 8-ring channels. It is also reflected in an increase in the accessibility of the OH groups in the 8-ring channels for the *n*-hexane molecule in the originally inaccessible pores (see the FTIR analysis par. 3.1.2). In the 2nd series, the mean pore diameter of the

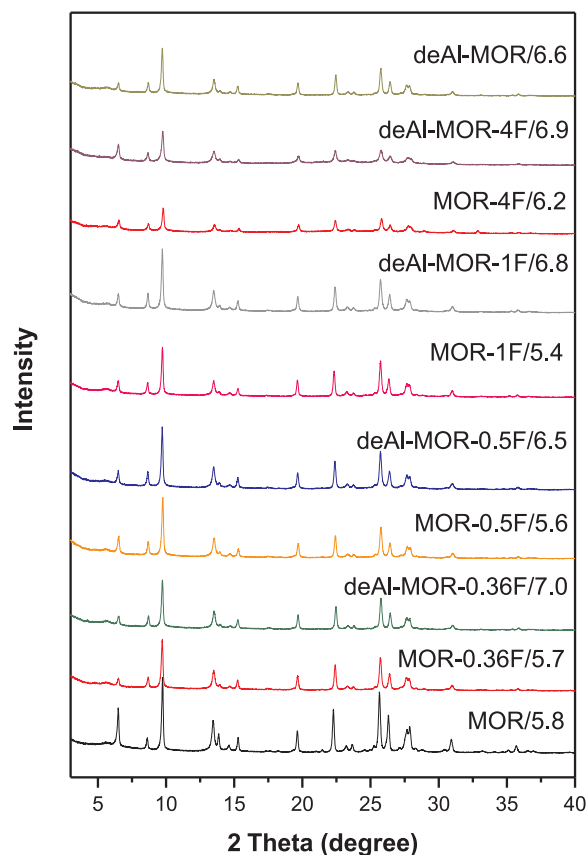


Fig. 3. XRD patterns of prepared MOR samples.

micropores is also increased. A procedure using the fluorination-alkaline treatment was developed by Yu et al. [20] to form a micro-mesoporous structure in the ZSM-5 zeolite with relatively high content of Al

Table 1Preparation and textural properties of fluorinated Al-rich mordenites determined by adsorption of N₂ and Ar at the temperature of liquid nitrogen.

Sample	Synthesis	Si/Al ^a	V _{MI} ^b (cm ³ ·g ⁻¹)	V _{ME} ^c (cm ³ ·g ⁻¹)	S _{EXT} (m ² ·g ⁻¹)
MOR/5.8	H-MOR parent	5.8	0.16	0.02	23
MOR-0.36F/5.8	0.36 M NH ₄ F + 0.2 M NaOH	5.7	0.21	0.04	40
deAl-MOR-0.36F/7.0	0.36 M NH ₄ F + 0.2 M NaOH + 0.1 M HNO ₃	7.2	0.21	0.05	51
MOR-0.5F/5.6	0.5 M NH ₄ F + 0.4 M NaOH	5.6	0.20	0.05	63
deAl-MOR-0.5F/5.6	0.5 M NH ₄ F + 0.4 M NaOH + 0.1 M HNO ₃	6.5	0.23	0.06	57
MOR-1F/5.4	1 M NH ₄ F + 0.4 M NaOH	5.4	0.12	0.06	65
deAl-MOR-1F/6.8	1 M NH ₄ F + 0.4 M NaOH + 0.1 M HNO ₃	6.8	0.24	0.06	68
MOR-4F/6.2	4 M NH ₄ F + 0.4 M NaOH	6.2	0	–	–
deAl-MOR-4F/6.9	4 M NH ₄ F + 0.4 M NaOH + 0.1 M HNO ₃	6.9	0.12	–	18
deAl-MOR/6.6	0.1 M HNO ₃	6.6	0.15	0.04	44

^a From chemical analysis.^b estimated from BdB *t*-plot method.^c V_{meso} = V_{total} - V_{micro}.

in the framework Si/Al ~ 15. The introduction of NH₄F into microporous ZSM-5 zeolite leads to the formation of F-bearing tetrahedral Al species which are readily dislodged in the subsequent alkaline treatment [20], leading to concurrent extraction of Al and Si. In our previous study [9], we demonstrated the development of secondary mesoporosity and preservation of microporosity via concurrent extraction of SiO₂ and a smaller amount of Al using the fluorination-alkaline treatment of MOR zeolite Si/Al ~ 12. The significant increase in the micropore volume, the increase in the size of some micropores and only minor formation of mesopores observed for the samples in series 1 and 2 prepared from Al-rich MOR (Si/Al ~ 5.8) show that a high concentration of Si-O-Al in the framework increases the resistance to alkaline treatment, as also reported for ZSM-5 [21]. The degree of susceptibility of the parent MOR/5.8 zeolite towards alkaline leaching after fluorination results in controlled concurrent extraction of both Al and Si atoms, indicated by comparable Si/Al compositions before and after leaching (Table 1), leading to desirable development of the microporosity without excessive formation of mesopores. The effect of the extraction of two neighbouring Al and Si atoms from the walls of the zeolite channels of MOR zeolite on the micropore structure is illustrated in Fig. 6A (for analysis of the local changes in the structure, see par. 3.1.2). It is obvious that the simultaneous extraction of Al and Si pairs from the MOR framework leads to enlargement and interconnection of the micropores (Fig. 1 and 2).

The fluorination-alkaline treatment with a concentration of 1 M NH₄F resulted in a decrease in the micropore volume compared to the parent zeolite, but the subsequent mild acid leaching increased the micropore volume to 0.24 cm³·g⁻¹. The preserved lattice fringes in the HR-TEM images and the intensity of the X-ray diffraction pattern of the zeolite after the fluorination-alkaline treatment are indicative of the preservation of the crystalline structure. Previous studies showed that hydrolysis of framework Al under harsh conditions of desilication leads to the formation of extraframework Al species which can easily block the openings in the pseudo-monodimensional channel structure of MOR [9,22]. A slight increase in the molar Si/Al ratio (Table 1) and the significant increase in the micropore volume after mild acid leaching indicate that the extraframework Al blocking part of the micropores was removed. The size distribution of the micropores indicates a further increase in their dimensions associated with supermicroporosity and 3D interconnection of the monodimensional mordenite channels [8,10,11,14,23].

The harshest fluorination treatment by 4 M NH₄F in the 4th series led to partial destruction of the crystalline structure, manifested in a significant decrease in the XRD intensity, negligibly low adsorption of N₂ in fluorination-alkaline treated sample MOR-4 F/6.2 and only partial restoration of the micropore volume of deAl-MOR-4 F/6.9 after mild acid treatment (Table 1). The 5th series was prepared by acid treatment of MOR/5.8 providing mildly dealuminated deAl-MOR/6.6. The size

distribution of the micropores determined by Ar adsorption clearly show their enlargement compared to MOR/5.8. The increase in the sizes and improvement of the connectivity of the micropore channels resulting from the extraction of Al from the framework have been described in the literature [23–25]. An addition to these desirable structural changes, a small decrease in the micropore volume could indicate the partial blockage of some micropores.

The adsorption measurements supplemented by the HR-TEM images and the X-ray diffractograms show the concurrent extraction of Al and Si by fluorination-alkaline-acid treatment of Al-rich MOR essentially alters the monodimensional structure with poorly accessible side pockets into a supermicropore channel structure characterised by high micropore volume (up to 0.25 ml·g⁻¹) formed by accessible internal voids with mean diameter of about 7.5 Å.

3.1.2. Concentration, nature and accessibility of acid sites in supermicroporous mordenites

3.1.2.1. Al MAS NMR analysis. Fig. 7 compares the ²⁷Al MAS NMR spectra of MOR zeolites before and after fluorination-alkaline-acid (Series 1–3) and acid (Series 5) treatments. A symmetric signal at 56 ppm associated with tetrahedrally coordinated aluminium (Al_{Td}) in the zeolite framework is observed in the ²⁷Al MAS NMR spectrum of the parent MOR/6 sample. The high symmetry of the signal is a result of the symmetrical local environment of the tetrahedral framework Al sites in the hydrated zeolite mitigating the quadrupolar couplings. The postsynthesis fluorination-alkaline and acid leaching lead to a broadening and shift in the maxima of the main signal to approx. 54 ppm, the formation of an asymmetric signal of high intensity at about 40 ppm, a barely visible signal of weak intensity at 30 ppm, and the appearance of a signal at 0 ppm. The shift in the maximum of the signal of the T_d coordinated Al is an indication of the preferable extraction of Al atoms located in specific T sites. This interpretation is consistent with previous studies of the acid leaching of MOR zeolites, which exhibited preferential dealumination of the T4 site [18,26,27]. In the literature [7,9,28–34], the signal at about 40 ppm is ascribed to perturbed Al in the framework in a less ordered environment and/or Al species partly removed from the framework. The combination of ²⁷Al (¹H) REDOR (3Q) MAS NMR and ²⁷Al (¹H) CP (3Q) MAS NMR experiments and DFT/Molecular computations in our previous study [30] showed that the shoulder at 40 ppm is associated with a perturbed framework Al in the (SiO)₃AlOH groups (δ_i = 59–62 ppm, C_Q = 5 MHz, and η = 0.3 – 0.4). The low local symmetry of the group results in the appearance of a highly asymmetric signal visible as a shoulder on the main signal. The weak signal observed around 30 ppm was assigned to traces of penta-coordinated extra-framework Al species [17]. The signal at 0 ppm is associated with octahedrally coordinated extra-framework Al. The perturbed framework tetrahedrally coordinated Al, the penta-coordinated and tetrahedral extra-framework Al manifested in the

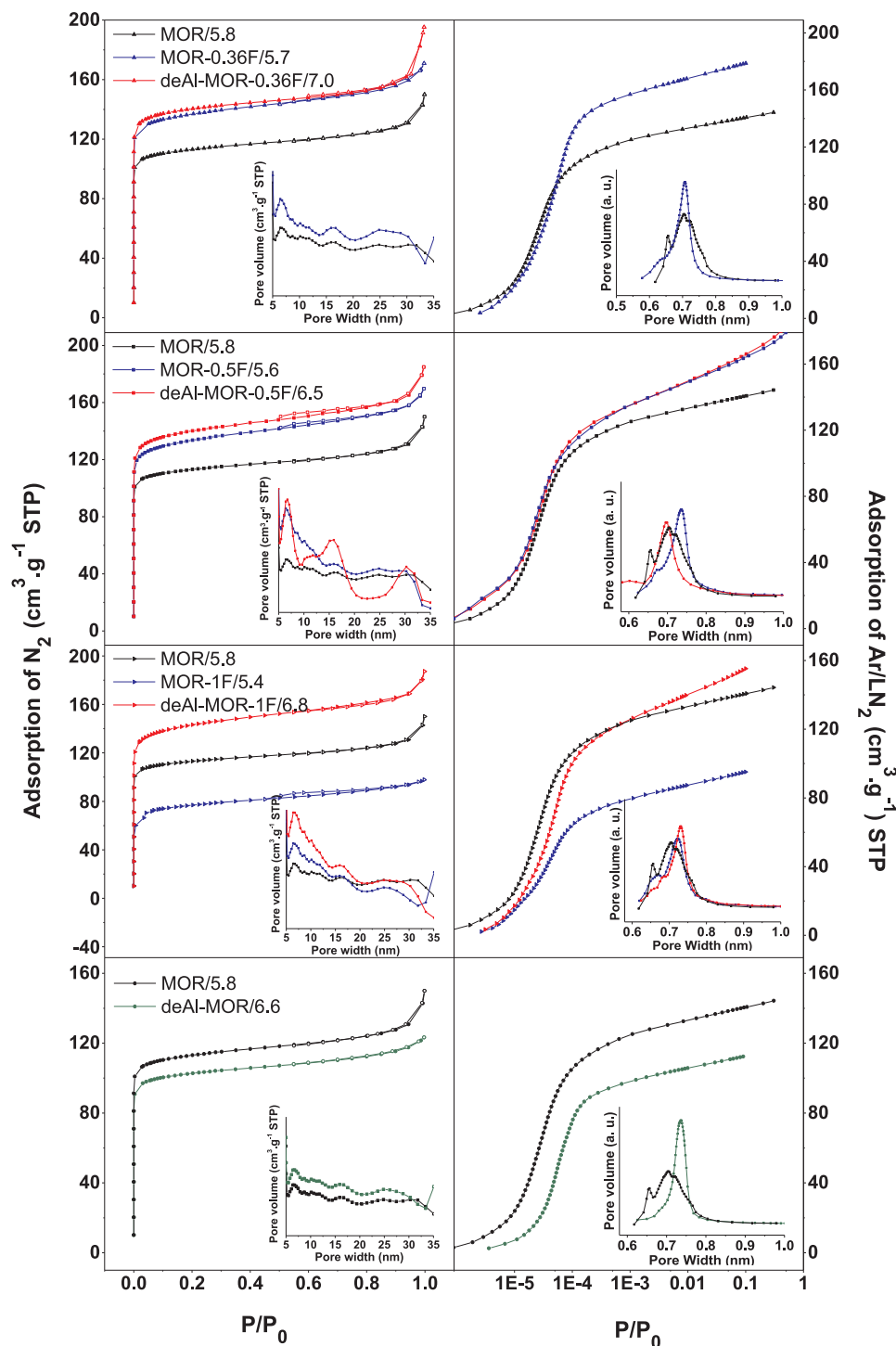


Fig. 4. Adsorption of N_2 and Ar/LN_2 at 77 K and detail of distribution of microporous and mesoporous structure before and after fluorination-alkaline-acid treatments (Series I - III), and also simple acid (Series V) treatment.

shoulder at 40 ppm and the signals at 30 and 0 ppm, respectively, were often observed in faujasite or high-silica zeolites after steaming [32–37]. The penta-coordinated and octahedral extra-framework Al could be present in the form of positively charged oxo/hydroxo moieties ($AlO^+ \cdot nH_2O$, $AlOH^{2+} \cdot nH_2O$) compensating the negative charge of the MOR framework or neutral $Al(OH)_3 \cdot nH_2O$, $Al_2O_3 \cdot nH_2O$ or $AlOOH \cdot nH_2O$ species (Fig. 5) [38]. The changes observed in the spectra after the fluorination-alkaline treatment are thus associated with partial extraction of Al preferentially from the T4 sites in the framework, the formation of a significant proportion of perturbed

framework Al in the $(SiO)_3AlOH$ groups and the formation of a limited amount of extra-framework Al species of various structures. Comparison of the ^{27}Al MAS NMR spectra of the samples from series 1 to series 3, prepared with increasing concentrations of the agents used for fluorination-alkaline treatments (Fig. 7), reveals a considerable increase in the intensity of the shoulder at about 40 ppm and broadening of the signal at 0 ppm with increasing harshness of the treatment, indicative of an increase in the proportion of the perturbed framework Al in the $(SiO)_3AlOH$ groups and greater distortion of the local environment of the extra-framework Al species, respectively.

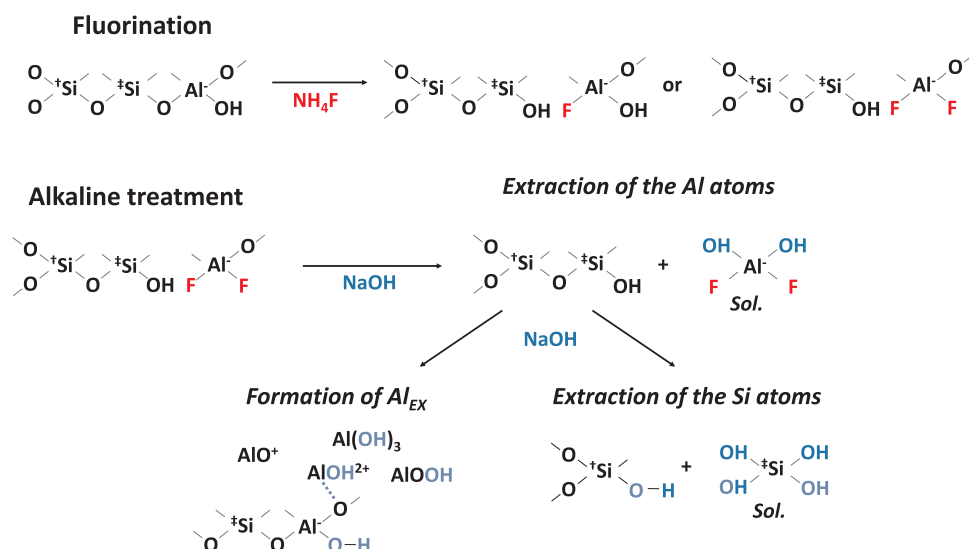


Fig. 5. Illustration of mechanism of the simultaneous extraction of Al^{3+} and Si^{4+} atoms and formation of the extraframework Al species by alkaline treatment of fluorinated Al-rich mordenites.

Similar changes in the ^{27}Al MAS NMR spectra of MOR/5.8 after acid leaching (deAl-MOR/6.6, Series 5.) and observed after fluorination-alkaline treatments (Series 1–3) indicate the formation of similar Al species after both the fluorination-alkaline treatment and the acid treatments. The decrease in the Al concentration (Table 1) and decrease in the intensity of the bands of the perturbed and extra-framework Al in the spectra of the acid-treated deAl-MOR-0.36 F/7.0 sample compared to MOR-0.36 F/5.7 (series 1) clearly show that the acid leaching results in concurrent dislocation of the framework Al and extraction of all the defective forms of the Al species from the zeolite. The gradual dislocation and extraction of Al from the zeolite framework and related structural changes in the MOR zeolites following acid treatment have been described in detail in the scientific literature [23–25].

3.1.2.2. FTIR analysis. Fig. 8 depicts the FTIR spectra of MOR zeolites before and after fluorination-alkaline-acid treatment (Series 1–3), and also simple acid (Series 5) treatments, as manifested before and after d_3 -acetonitrile adsorption experiments. The spectra of the samples of all the series display a typical asymmetrical shape of the band in the OH region with a dominant band at 3610 cm^{-1} and a clearly defined sideband at lower wavenumbers. This shape of the spectra, characteristic for MOR, was already explained by Wakabayashi et al. [39] and Zholobenko et al. [40] and assigned to an OH bond located in the main 12-ring channels, and the low-frequency component near 3590 cm^{-1} was attributed to OH in the smaller side pockets with an 8-ring, and connected with the T3 site [39]. Further analysis substantiated this interpretation and some effort was devoted to use this analysis for semi-quantitative evaluation of both structures. Despite some controversies in this respect, we used the recommendation of Makarova [40] for the semi-quantitative evaluation, yielding a ratio of extinction coefficients of the 12 OH / 8 OH bands of about 1.5. Semi-quantitative analysis of the acidity of the analyzed samples was based on the results of the d_3 -acetonitrile adsorption experiments, using the extinction coefficient for d_3 -acetonitrile interacting with the Lewis acid sites as $\epsilon_L = 3.60\text{ cm}\cdot\mu\text{mol}^{-1}$, and $\epsilon_B = 2.05\text{ cm}\cdot\mu\text{mol}^{-1}$ for d_3 -acetonitrile interacting with the OH [16].

The FTIR spectra of the parent MOR/5.8 sample represent typical spectra of well-developed MOR zeolites with relatively high-intensity bands in the region of the Brønsted OH, with a dominant band at 3610 cm^{-1} , i.e. at the position of OH located in the 12-ring, and the relatively less intense side band at 3590 cm^{-1} of the OH in the 8-ring. Based on the quantitative analysis, the relative contents of the two 12 OH / 8 OH structures in the parent zeolite equaled about 2. The small

intensity of the band of the terminal OH (a band at about 3745 cm^{-1}) and negligible structure indicated at the position typical of AlOH with the band at 3660 cm^{-1} further demonstrated the regularity of the parent MOR. The results of the adsorption of d_3 -acetonitrile provided data for semi-quantitative evaluation of the Brønsted (a band at 2286 cm^{-1}) and two distinguished Al-related Lewis acid sites (with bands at 2313 and 2323 cm^{-1}). Analysis of the spectra in the OH region demonstrated that, after the d_3 -acetonitrile adsorption/partial desorption procedure, most of the terminal SiOH were free of the d_3 -acetonitrile while, at the same time, full interaction with both the OH groups located in the 12-ring and 8-ring was achieved. Accordingly, the d_3 -acetonitrile spectra could have been used for the semi-quantitative analysis of the concentration of both OH and the Lewis sites. The relatively intense additional band at 2280 cm^{-1} with a shoulder at about 2277 cm^{-1} was assigned to the d_3 -acetonitrile molecule interacting with structurally undefined defects in the MOR structure and a small part of the terminal SiOH, which was not fully reconstructed during the mild desorption of the d_3 -acetonitrile. It should be noticed that the band at 2280 cm^{-1} was much less intense in the previous experiments over MOR (Si/Al ~ 12) with lower Al content in the previous study [8].

Generally, all the MOR samples after the postsynthesis fluorination-alkaline and acid leaching displayed some uniform features with a decrease in the total OH bands and well-expressed change in the relative ratio of the 12/8-ring structures. For all the samples, the treatments led to a steep increase in the intensity of the Lewis band at about 2323 cm^{-1} . It seemed significant that both the acid (Series 5) and combined treatments (Series 1–4) induced elimination of the 2280 cm^{-1} band, assigned to unspecified defect structures present in the parent zeolite.

Some indication on the presence and relative concentration of the AlOH structures indicated by the IR band in the 3660 cm^{-1} region could be gained, suggesting the formation of this structure after the combined treatment and not fully regularly decreasing again after acid treatment. These results are to some extent consistent with previous studies on the acid leaching of MOR zeolites, which indicated preferential dealumination of the T4 site connected to the 12-ring [18,26,27] and accordingly relatively higher stability of the 8-ring sites, connected with the T3 site [41]. The same could be indicated for the formation of the perturbed Al species, connected either to the Al-related Lewis positions or to the AlOH structure. All these structures could be regarded as perturbed Al sites in the framework in a less ordered environment and/or Al species partly removed from the framework.

The changes in the FTIR spectra observed either before or after the d_3 -acetonitrile adsorption/desorption cycle of the samples exposed to

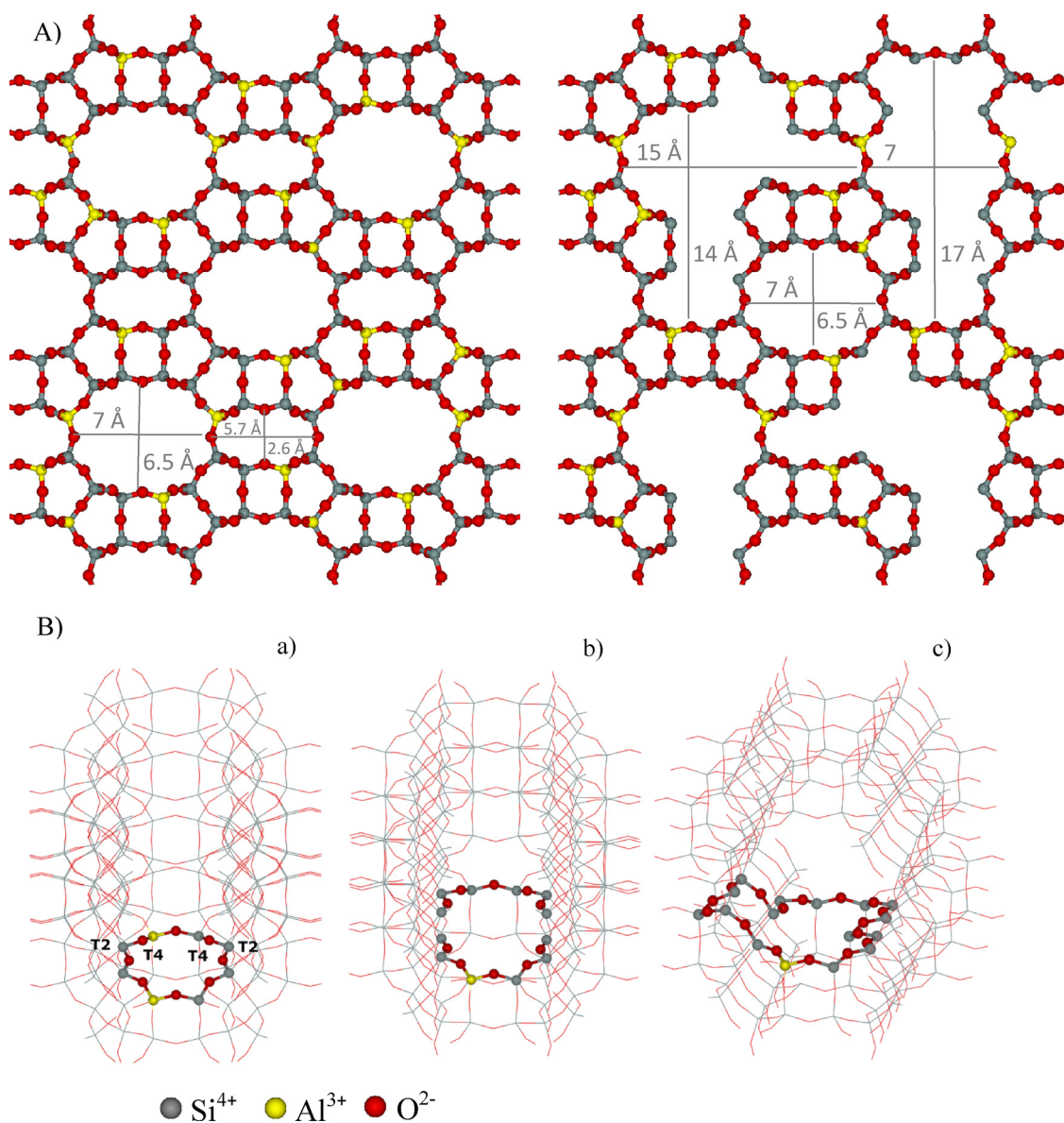


Fig. 6. Schematic illustration of mordenite openings before and after extraction of Si and Al by fluorination-alkaline-acid treatments. A) Illustration of pore size changes and B) structure of the 8-ring a) before the treatment and an illustration of the changes in local arrangements after extraction of Al from the T4 site and a neighbouring Si atom from b) the T2 or c) the T4 site.

fluorination-alkaline treatment thus indicate partial extraction of Al from the framework preferentially from the 12-ring sites and formation of perturbed framework Al groups and some amount of extra-framework Al species, including Al-related Lewis species. Increasing the concentrations of the agents used for fluorination-alkaline treatments (Fig. 8) led to an increase in the Al elimination process going from Series 1 to 3. The changes in the spectra of the MOR in Series 5 were rather similar, indicating similar production of Al species after both fluorination-alkaline treatment and acid treatments but with much smaller formation of the (SiO)₃AlOH groups after acid treatment.

3.1.3. Summary of structural features of supermicroporous mordenites

The structural changes in mordenites induced by a partial dealumination using mineral acids were described at a molecular level by Van Geem [18] and others [27]. Preferential removal of aluminium from the labile T4 site in the 4-ring forming the walls of the main 12-ring channels results in widening of part of the 8-ring channels and the creation of new interconnections between the main channels [8,18,27]. However, a small microporous volume (Table 1) and low accessibility

of the OH groups for *n*-hexane (Table 2) in the mildly dealuminated deAl-MOR/6.6 sample indicate that the desirable changes in the channel structure require the removal of larger proportions of Al from the framework. ²⁷Al MAS NMR analysis (Fig. 7) and the adsorption measurements (Table 1) clearly showed that the acid treatment does not extract all the atoms removed from the framework and various extra-framework species partly block the pores. In contrast, the fluorination-alkaline-acid treatment (series I – 3) leads to a much larger increase in the volume of the supermicropores when a similar amount of Al is extracted from the zeolites (compare, e.g., V_{MI} 0.15 and 0.24 cm³.g⁻¹ for deAl-MOR/6.6 and deAl-MOR-1 F/6.8, respectively). The chemism of the concurrent extraction of Al and Si atoms from the zeolite framework by fluorination-alkaline treatments, as described by Yu et al. [20], is shown in Fig. 5. After fluorination, a fraction of Si-O-Al framework entities is cleaved by the incorporation of fluorides, but the attacked Al sites are still integrated within the framework as F-bearing tetrahedral Al species [20]. The F-bearing Al are extracted from the zeolite in the form of [AlF₂(OH)₂]-Na⁺ together with the neighbouring Si atoms during the subsequent alkaline leaching (Fig. 5). Fig. 6B shows

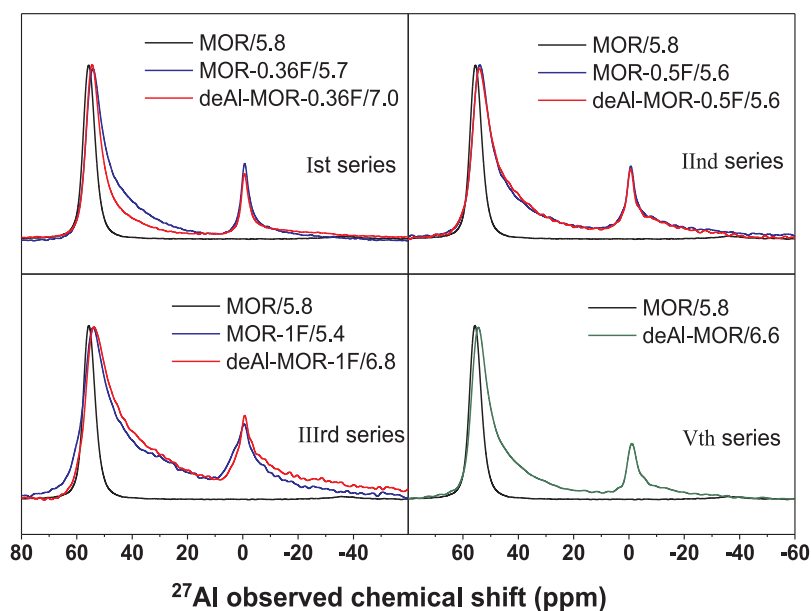


Fig. 7. ^{27}Al MAS NMR spectra for hydrated mordenite zeolites after fluorination-alkaline-acid treatments (Series I - III), and also simple acid (Series V) treatment.

an illustration of the changes in the local arrangements of the 8-ring after extraction of Al from the T4 site and a neighbouring Si atom from the T2 or T4 site. Although we do not have data showing the dislocation of specific T-atoms, the illustration is in a good agreement with the textural data (Table 1) and the extraction of Al from the framework preferentially from the 12-ring sites is confirmed by the FTIR spectra either before or after the d_3 -acetonitrile adsorption.

The changes in the microporous volume, the micropore size and the accessibility of the acid with the chemical conditions of the fluorination-alkaline leaching (Tables 1 and 2) indicate that the proportion of the extracted atoms is controlled by the interplay of the concentration/distribution of Al in zeolite and the conditions of the treatment. The high intensities in the signals at 30 and 0 ppm in the ^{27}Al MAS NMR spectra reflect the large content of the penta-coordinated and octahedral extraframework Al in the samples prepared using the highest concentrations of the fluorination agent ($\geq 1 \text{ M NH}_4\text{F}$). Subsequent acid leaching of MOR-1F/5.4 using 0.1 M HNO_3 (deAl-MOR-1F/6.8) resulted in a slight increase in the molar Si/Al ratio and a significant increase in the microporous volume from 0.12 to 0.24 cm^3g^{-1} (Table 1), as well as a slight increase in the concentration of Brønsted sites from 0.22 to 0.24 mmol g^{-1} and Lewis sites from 0.71 to 0.81 mmol g^{-1} (Table 2). These findings indicate that the extraframework Al species formed in the channels after the fluorination-alkaline treatment and blocking part of the micropores were removed by acid leaching. The principle of the fluorination-alkaline-acid treatment is similar to the coupling of dealumination with desilication employed for flexible tailoring of the concentration of aluminium related acid sites in microporous zeolites [7,8,28,42]. The uniqueness of the fluorination-alkaline-acid procedure lies in the effective formation of 3D connected supermicroporous channels enhancing the accessibility of the acid sites without the formation of a significant proportion of the secondary mesoporosity (V_{MI} up to 0.25 cm^3g^{-1} , the mean pore size $\sim 7.5 \text{ \AA}$).

3.1.4. Structure of platinum

The platinum loaded in the amount of 1.5 wt. % in the form of well-dispersed metallic clusters was shown to guarantee the hydrogenation-dehydrogenation function under the employed reaction conditions and the formation of hexane/hexene according to the thermodynamic equilibrium [8,9]. The hydroisomerisation under these conditions is controlled by the acidic functions of the bi-functional Pt/H-MOR

catalysts [43,44]. Accordingly, the dispersion and the state of Pt was analysed using complementary HR-TEM and the adsorption of CO followed by FTIR. The HR-TEM images in Fig. 9B indicate smoothly distributed nanoparticles with a size up to 2–3 nm. Also the occurrence of a minor fraction of platinum clusters with a wide distribution in the size range of 3–40 nm was observed on the external surface of the zeolite crystals. The FTIR spectra of adsorbed CO on reduced Pt/H-MOR were characterised by a dominant adsorption band at 2080 cm^{-1} , reflecting the stretching mode of linearly adsorbed CO on the reduced Pt^0 in metallic clusters of 1–20 nm in size [45,46]. The reduced form of platinum is also confirmed by the absence of any significant absorption intensity at about at 2180–2130 cm^{-1} characteristic of adsorbed CO on Pt^{2+} ions or $\text{Pt}_n\delta^+$ clusters [45,46].

3.2. Hydroisomerisation of *n*-hexane

Fig. 10 shows the hydroisomerisation activity over the series of MOR zeolites after fluorination-alkaline and subsequent acid treatments. The catalytic activity is expressed as the yield of the branched C_6 species (the sum of all the di-branched 2,2- and 2,3-dimethylbutanes and mono-branched 2- and 3-methylpentanes) in dependence on the reaction temperature. The selectivity is reflected in the yields of all the C_1 – C_5 cracking by-products as the cracking took place in parallel with isomerisation at higher temperatures. The yields of the individual branched hexane isomers and lower molecular weight by-products for hydroisomerisation of *n*-hexane over all the prepared Pt/H-MOR at 225 °C and 250 °C are given in Table 3.

Over the parent Pt/H-MOR/5.8, a very low yield of *iso*- C_6 isomers first appeared at 150 °C, (see Fig. 10A), and then their yield continuously increased up to approximately 44% at 275 °C, and finally decreased again (as a result of unselective cracking reactions, which began to take place at 250 °C and then increased continuously to high temperatures, see Fig. 10 B). Thus the yield of *iso*- C_6 finally attained values below 23% at 325 °C. The fluorination-alkaline treatments of the parent MOR under mild conditions in the 1st series resulted in a substantial increase in its activity and the isomer yield was improved by more than two-fold in the broad temperature range 175–250 °C. Further, the subsequent mild dealumination led to a further increase and the resultant *iso*- C_6 yield exceeded 62–63% of branched isomers at temperatures of 225–250 °C. The corresponding cracking was analogously elevated at temperatures above 250 °C (see Fig. 10 B). In the 2nd

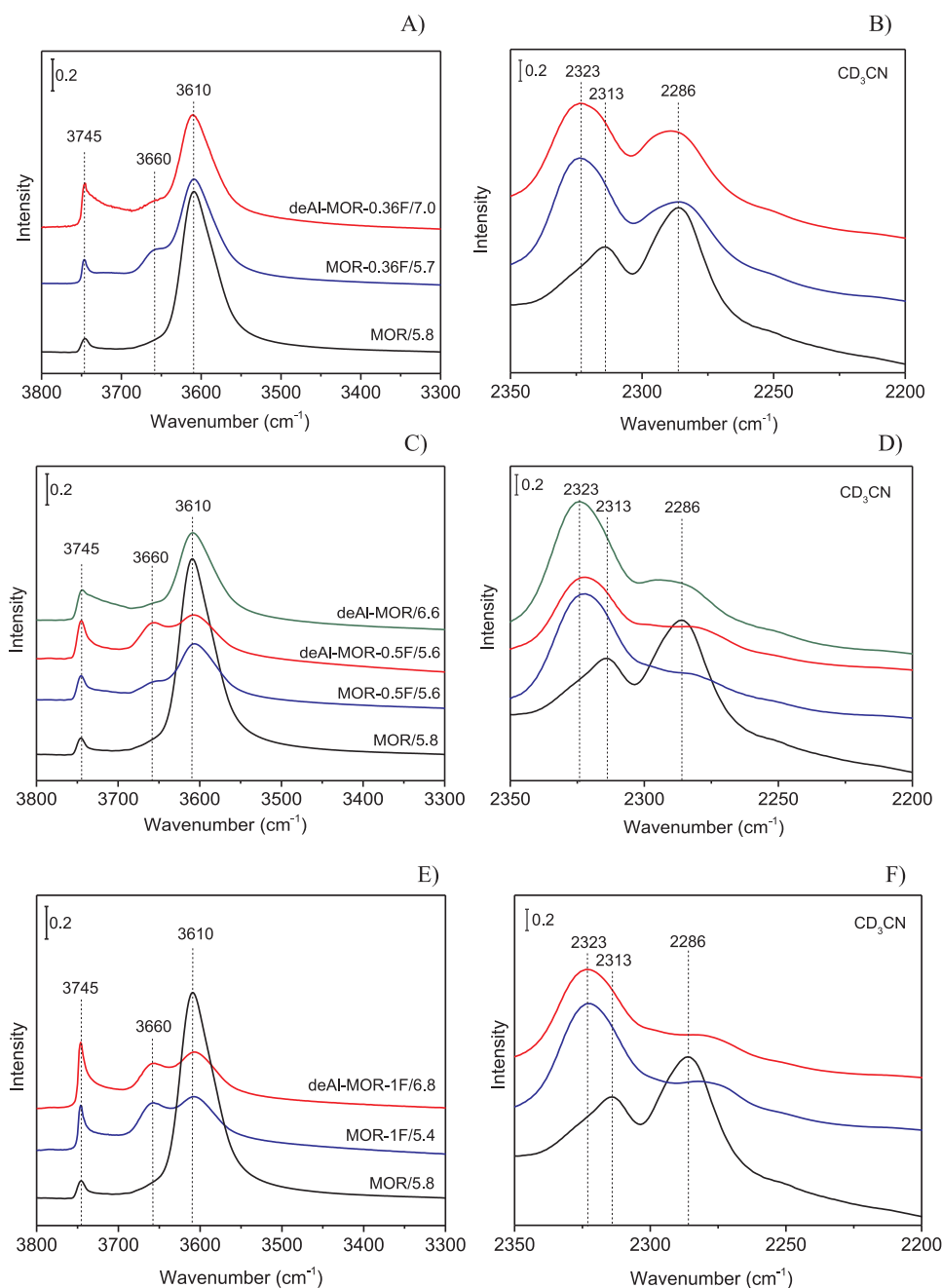


Fig. 8. Comparison of FTIR spectra of adsorbed d_3 -acetonitrile (B, D, and F) and the OH stretching region (A, C, and E) for mordenite zeolites after fluorination-alkaline-acid treatments (Series I - III), and acid (Series V) treatment. A), B) Series I; C, D) Series II and V, and E, F) Series III.

series (Fig. 10 C, D) the slightly stronger fluorination followed by stronger alkali treatment compared to Series 1 and the mild acid dealumination of the MOR increased the catalyst activity even further and 66% *iso*-C₆ yield was obtained at T < 250 °C, over both fluorination-alkaline-acid treated catalysts. Substantially stronger fluorination in series 3 (Fig. 10 E, F) followed by mild dealumination finally brought the highest isomer yield increase up to 72%, which was obtained at a temperature as low as 225 °C. All the improved isomer yields were also accompanied by increased cracking yields of C₁ - C₅ by-products, their values increased approximately 3–4 times compared to the parent/microporous MOR, e.g. the yield increased from approximately 4% to 15%, from the parent to the last fluorination-alkaline-acid treated MOR, respectively, at 250 °C and continued to predominate at the highest temperatures.

The strongest fluorination-alkaline treatment of 4 M NH₄F in 4th

series caused a dramatic drop in the yield of isomers (shown in Fig. 10 G, H), although a slight improvement with mild dealumination was found, nevertheless not achieving the original activity of the parent MOR. In this case, the formation of by-products was proportionately suppressed. Thus, using the optimal fluorination-alkaline-acid step sequence in series 3, a resultant highest yield of C₆-isomers as high as 72% was achieved at a temperature of 225 °C, compared to 44% at 275 °C achieved for the parent MOR. For comparison, only a 55% yield at 250 °C was achieved on dealuminated deAl-MOR/6.6 (Series 5) with a corresponding increase in the amount of by-products from 4% to 12% at 250 °C (shown in Fig. 10 I, J).

Summing up, the mordenite zeolites with the 3D connected super-microporous channels provide much higher yields of branched isomers in the hydroisomerization reaction. The high activity is unequivocally linked to enhancement of accessibility of the active sites and molecular

Table 2
Concentrations of bridging hydroxyls and Brønsted and Lewis sites in zeolite and accessibility of OH groups in fluorinated Al-rich mordenites.

Sample	Si/Al ^a	c _{Al} ^a	c _B ^b	c _L ^c	c _{B+2L} ^d	Accessibility of OH groups ^e (%)
MOR/5.8	5.8	2.31	0.97	0.45	1.86	19
MOR-0.36F/5.8	5.7	2.51	0.37	0.81	1.99	48
deAl-MOR-0.36F/7.0	7.2	2.05	0.55	0.75	2.04	51
MOR-0.5F/5.6	5.6	2.55	0.22	0.81	1.85	54
deAl-MOR-0.5F/5.6	6.5	2.24	0.17	0.47	1.11	78
MOR-1F/5.4	5.4	2.65	0.22	0.71	1.64	64
deAl-MOR-1F/6.8	6.8	2.16	0.24	0.80	1.83	59
deAl-MOR/6.6	6.6	2.22	0.32	0.96	2.25	24

^a From chemical analysis.

^b Concentrations of acid Brønsted and Lewis sites, respectively, from FTIR spectra of adsorbed *d*₃-acetonitrile.

^c Concentrations of acid Brønsted and Lewis sites, respectively, from FTIR spectra of adsorbed *d*₃-acetonitrile.

^d Concentration of Al estimated from the concentration of Brønsted and Lewis sites (c_{Al} = c_B + 2c_L).

^e From FTIR spectra of the bridging OH groups after adsorption of *n*-hexane.

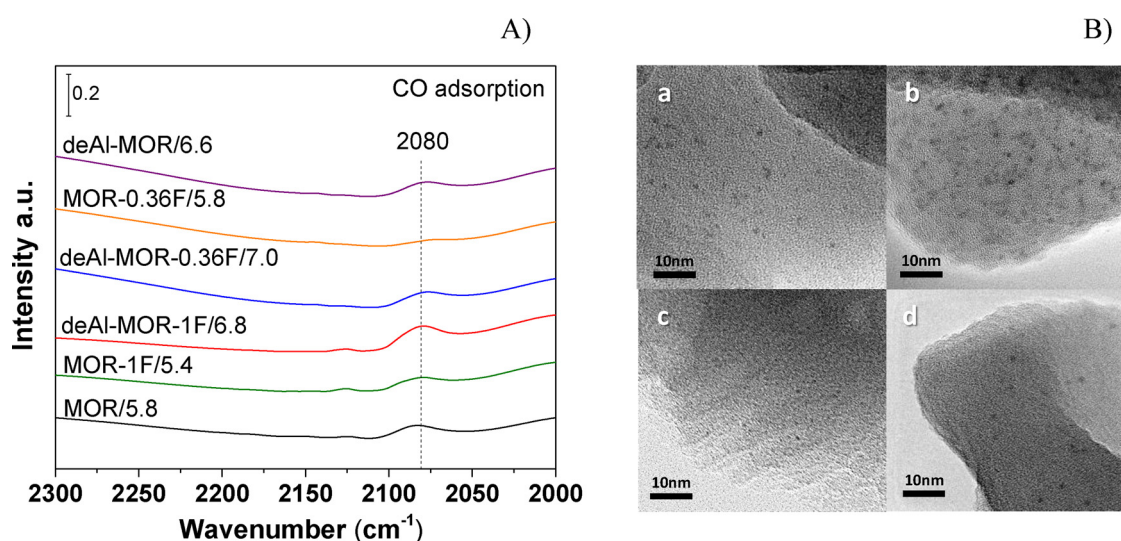


Fig. 9. A) Typical FTIR spectra of CO adsorbed on Pt/H-MOR zeolites reduced by hydrogen at 250 °C and B) characteristic TEM images of Pt in Pt/H-MOR catalysts, of a) parent MOR/5.8, b) MOR-1 F/5.4, c) deAl-MOR-1 F/6.8 and d) deAl-MOR/6.6.

transport in an environment of nonrestricted microporous channels. However, we can not exclude that the increase in the yield of branched isomers and corresponding specific activity is also associated with contributions from others synergistic effects. The presence of electron acceptor Lewis sites in zeolites can contribute to the enhancement of catalytic activity, as demonstrated in the literature for numerous hydrocarbons [47–50]. The significant concentrations of the Lewis sites were observed in the FTIR spectra of adsorbed *d*₃-acetonitrile (Fig. 8 and Table 2) and the presence of penta-coordinated and octahedral extraframework Al was obvious in the ²⁷Al MAS NMR spectra (Fig. 7) of the supermicroporous mordenites. An increased strength of the Brønsted sites next to Lewis sites [51,52] or additional polarization of reactants by a Lewis acid site adjacent to a Brønsted site [53,54] can contribute to the overall activity of the supermicroporous mordenites.

The stability of the yields and selectivity as a function of time-on-stream was analysed over the parent MOR/5.8 and over the resultant fluorination-alkaline-acid treated deAl-MOR-0.5 F/5.6 from Series 2 as a typical supermicroporous MOR zeolite (Fig. 11). The yield of all the isomers decreased slightly over the parent MOR/5.8, from 24% of the initial value to 21% after 48 h of continuous C₆-feeding at a reaction temperature of 235 °C. The conversion was observed to be nearly constant, i.e. 44–46%, over deAl-MOR-0.5 F/5.6 and the yields of the individual mono-branched (38–40%) and di-branched isomers (~ 6%) were also constant within > 48 h of time-on-stream at 210 °C. The

amount of (C₁ - C₅) by-products was below ~ 1% during both reaction runs. All these observations indicate sufficient structural stability and the absence of any substantial structural damage to the supermicroporous Pt/H-MOR under the reaction conditions; moreover, it also demonstrated some improvement in the time-on-stream stability compared with the untreated parent MOR/5.8.

4. Conclusions

We demonstrated that the simultaneous extraction of Al and Si from the Al-rich MOR framework using fluorination-alkaline-acid treatment leads to high micropore volume (up to 0.25 cm³.g⁻¹), enlargement of the micropores (with mean diameter of about 7.5 Å) and interconnection of the channels. The re-organisation of the mono-dimensional channel system of the MOR zeolite into a three-dimensional supermicroporous zeolite structure with connectivity of the pore network resulting in good accessibility to the acid sites allows the preparation of catalytic materials providing strongly enhanced hydroisomerisation properties. These findings highlight the essential role of the 3D supermicroporous structure in the catalytic activity, selectivity of the transformation of *n*-hexane into the corresponding branched isomers without excessive participation of consecutive cracking reactions, and long-term catalytic stability. The concept provides opportunities for the creation of accessible Brønsted and Lewis active sites in Al-rich zeolites

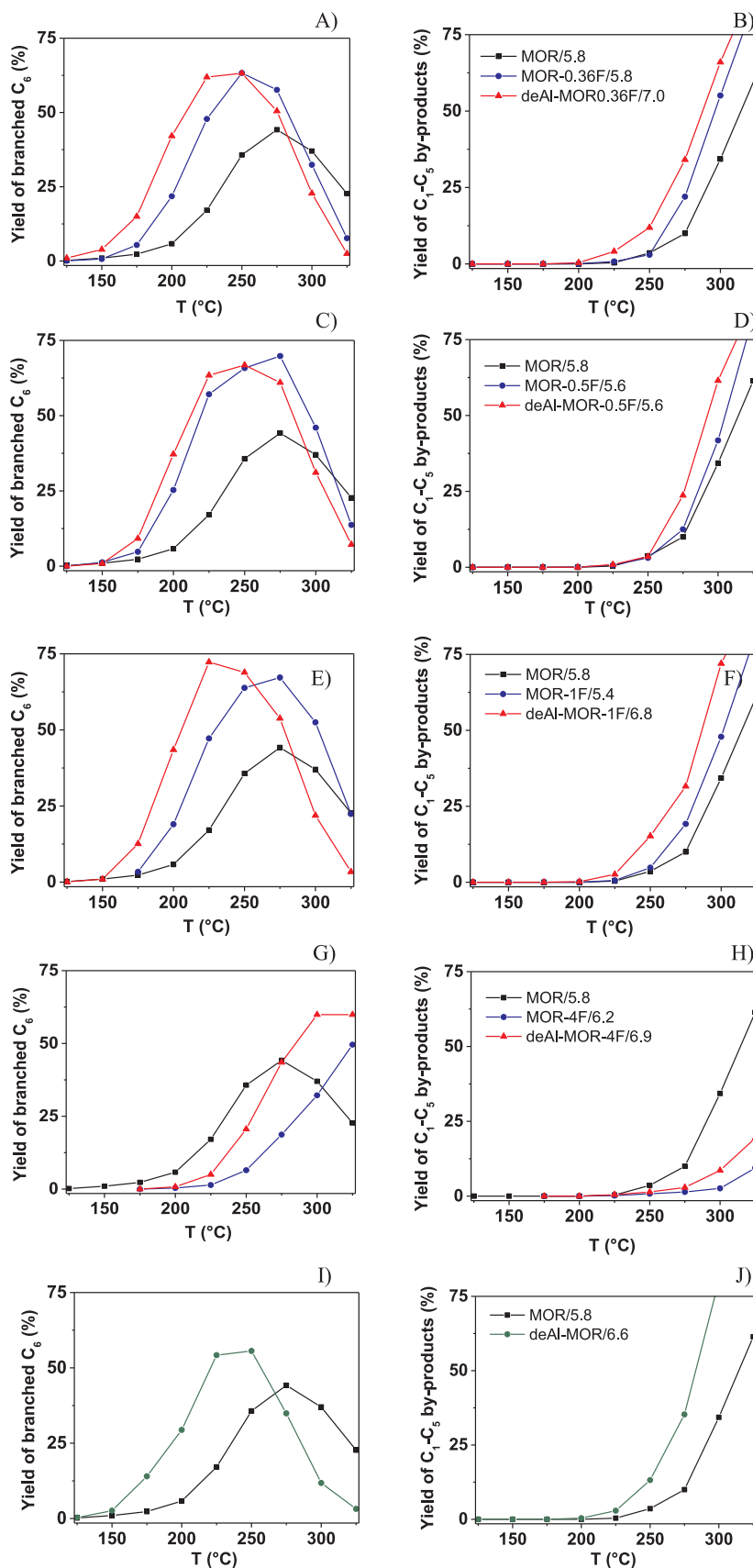
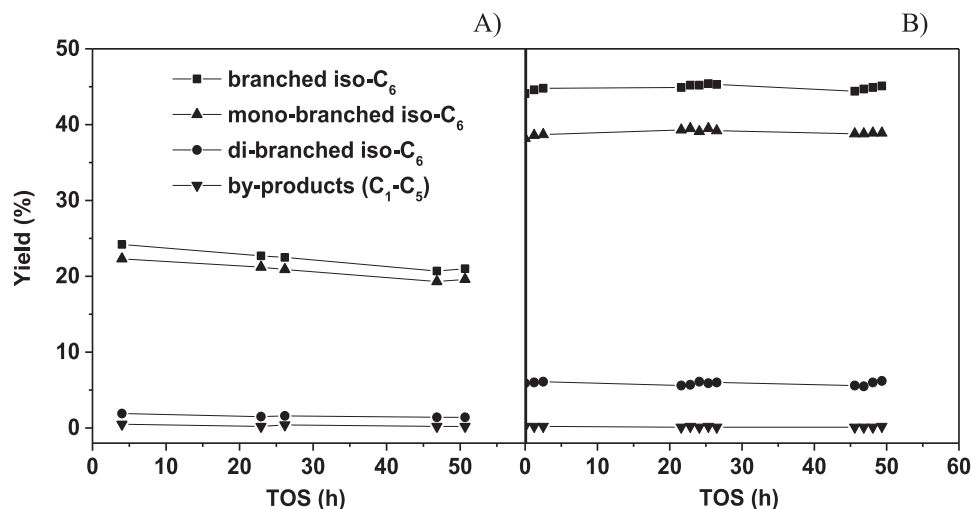


Fig. 10. The yields of branched C6 isomers and C1-C5 by-products in the hydroisomerization of *n*-hexane over Pt/H-MOR zeolites. A, B) Series I; C, D) Series II; E, F) Series III; G, H) Series IV and I, J) Series V.

Table 3Yields of branched hexane isomers and lower molecular weight by-products for hydroisomerization of *n*-hexane over Pt/H-MOR at 225 °C and 250 °C.

Sample	$\Sigma Y_{\text{iso-C}_6}$ (%)		2,2-DMB		2,3-DMB		2-MP		3-MP		C ₁ -C ₅ (%)	
	225 °C	250 °C	225 °C	250 °C	225 °C	250 °C	225 °C	250 °C	225 °C	250 °C	225 °C	250 °C
MOR/5.8	17.5	36.5	0.1	0.7	2.2	3.8	6.6	8.0	8.6	24.0	0.4	2.6
MOR-0.36F/5.8	47.8	62.1	3.5	6.5	5.7	7.2	9.4	9.8	29.2	38.6	0.8	7.4
deAl-MOR-0.36F/7.0	63.7	65.8	3.0	5.6	7.2	6.9	12.5	11.4	41.0	41.9	2.8	10.9
MOR-0.5F/5.6	57.1	65.8	2.0	5.1	6.4	7.0	10.9	12.1	37.8	41.6	0.7	3.1
deAl-MOR-0.5F/5.6	63.4	66.8	2.5	5.1	6.8	6.6	12.8	12.3	41.3	42.8	0.9	3.5
MOR-1F/5.4	32.8	49.7	0.5	1.8	3.6	5.3	8.5	10.0	20.2	32.6	0.6	4.8
deAl-MOR-1F/6.8	72.3	68.9	3.9	9.1	7.9	6.7	13.6	12.0	46.9	41.1	2.6	15.2
deAl-MOR/6.6	54.2	55.6	2.2	4.3	5.8	5.9	9.7	9.0	36.5	36.4	2.9	13.2
MOR-4F/6.2	1.4	6.5	0.0	0.0	0.0	0.3	0.8	3.5	0.6	2.7	0.2	0.8
deAl-MOR-4F/6.9	5.0	20.6	0.0	0.1	0.0	1.2	2.7	6.8	2.3	12.5	0.5	1.4

**Fig. 11.** The test of catalytic stability over A) microporous zeolite MOR/5.8 and B) supermicroporous deAl-MOR-0.5F/5.6 as a dependence of yields of the individual branched hexane isomers and C1-C5 by-products on time-on-stream in hydroisomerization of *n*-hexane.

for diffusion-restricted reactions.

Acknowledgments

This work was supported by the Grant Agency of the Czech Republic under project No. 15-12113S. The authors acknowledge the assistance provided by the Research Infrastructures NanoEnviCz (Project No. LM2015073) and Pro-NanoEnviCz (Project No. CZ.02.1.01/0.0/0.0/16_013/0001821), supported by the Ministry of Education, Youth and Sports of the Czech Republic.

References

- W. Vermeiren, J.P. Gilson, *Top. Catal.* 52 (2009) 1131–1161.
- H. Weyda, E. Köhler, *Catal. Today* 81 (2003) 51–55.
- D. Kaucký, B. Wichterlová, J. Dedecek, Z. Sobalik, I. Jakubec, *Appl. Catal. A* 397 (2011) 82–93.
- T. Løften, E.A. Blekkan, *Appl. Catal. A* 299 (2006) 250–257.
- S. Kuba, P. Lukinskas, R.K. Grasselli, B.C. Gates, H. Knözinger, *J. Catal.* 216 (2003) 353–361.
- A. Chica, A. Corma, *J. Catal.* 187 (1999) 167–176.
- P. Sazama, Z. Sobalik, J. Dedecek, I. Jakubec, V. Parvulescu, Z. Bastl, J. Rathousky, H. Jirglova, *Angew. Chem., Int. Ed.* 52 (2013) 2038–2041.
- J. Pastvova, D. Kaucky, J. Moravkova, J. Rathousky, S. Sklenak, M. Vorokhta, L. Brabec, R. Pilar, I. Jakubec, E. Tabor, P. Klein, P. Sazama, *ACS Catal.* 7 (2017) 5781–5795.
- P. Sazama, D. Kaucky, J. Moravkova, R. Pilar, P. Klein, J. Pastvova, E. Tabor, S. Sklenak, I. Jakubec, L. Mokrzycki, *Appl. Catal. A-Gen.* 533 (2017) 28–37.
- M. Tromp, J.A. van Bokhoven, M.T. Garriga Oostenbrink, J.H. Bitter, K.P. de Jong, D.C. Koningsberger, *J. Catal.* 190 (2000) 209–214.
- S.V. Konnov, I.I. Ivanova, O.A. Ponomareva, V.I. Zaikovskii, *Microporous Mesoporous Mater.* 164 (2012) 222–231.
- H. Chiang, A. Bhan, *J. Catal.* 283 (2011) 98–107.
- K.-j. Chao, H.-c. Wu, L.-j. Leu, *Appl. Catal. A* 143 (1996) 223–243.
- N. Viswanadham, L. Dixit, J.K. Gupta, M.O. Garg, *J. Mol. Catal. A Chem.* 258 (2006) 15–21.
- R.M. Barrer, *J. Chem. Soc. (Resumed)* (1948) 2158–2163.
- B. Wichterlova, Z. Tvaruzkova, Z. Sobalik, P. Sarv, *Microporous Mesoporous Mater.* 24 (1998) 223–233.
- J.A. Van Bokhoven, D.C. Koningsberger, P. Kunkeler, H. Van Bekkum, A.P.M. Kentgens, *J. Am. Chem. Soc.* 122 (2000) 12842–12847.
- P.C. Van Geem, K.F.M.G.J. Scholle, G.P.M. Van Der Velden, W.S. Veeman, *J. Phys. Chem.* 92 (1988) 1585–1589.
- P.A. Webb, O. Clyde, *Analytical Methods in Fine Particle Technology*, M.I. Corporation (Ed.), Norcross, GA 30093 U.S.A., 1997.
- L. Yu, S. Huang, S. Miao, F. Chen, S. Zhang, Z. Liu, S. Xie, L. Xu, *Chem. Eur. J.* 21 (2015) 1048–1054.
- J.C. Groen, J.A. Moulijn, J. Perez-Ramirez, *J. Mater. Chem.* 16 (2006) 2121–2131.
- P. Sazama, Z. Sobalik, J. Dedecek, I. Jakubec, V. Parvulescu, Z. Bastl, J. Rathousky, H. Jirglova, *Angew. Chem., Int. Ed.* 52 (2013) 2038–2041.
- N. Viswanadham, M. Kumar, *Microporous Mesoporous Mater.* 92 (2006) 31–37.
- M. Tromp, J.A. van Bokhoven, M.T. Garriga Oostenbrink, J.H. Bitter, K.P. de Jong, D.C. Koningsberger, *J. Catal.* 190 (2000) 209–214.
- A.N.C. Van Laak, S.L. Sagala, J. Zecevic, H. Friedrich, P.E. De Jongh, K.P. De Jong, *J. Catal.* 276 (2010) 170–180.
- M. Muller, G. Harvey, R. Prins, *Microporous Mesoporous Mater.* 34 (2000) 135–147.
- M.-C. Silaghi, C. Chizallet, J. Sauer, P. Raybaud, *J. Catal.* 339 (2016) 242–255.
- P. Sazama, B. Wichterlova, J. Dedecek, Z. Tvaruzkova, Z. Musilova, L. Palumbo, S. Sklenak, O. Gonsiorova, *Microporous Mesoporous Mater.* 143 (2011) 87–96.
- P. Sazama, B. Wichterlova, S. Sklenak, V.I. Parvulescu, N. Candu, G. Sadovska, J. Dedecek, P. Klein, V. Pashkova, P. Stastny, *J. Catal.* 318 (2014) 22–33.
- J. Brus, L. Kobera, W. Schoefberger, M. Urbanová, P. Klein, P. Sazama, E. Tabor, S. Sklenak, A.V. Fishchuk, J. Dedecek, *Angewandte Chem. – Int. Ed.* 54 (2015) 541–545.
- P. Sazama, E. Tabor, P. Klein, B. Wichterlova, S. Sklenak, L. Mokrzycki, V. Pashkova, M. Ogura, J. Dedecek, *J. Catal.* 333 (2016) 102–114.
- A. Samoson, G. Lippmaa, G. Engelhardt, U. Lohse, H.G. Jerschkewitz, *Chem. Phys. Lett.* 134 (1987) 589–592.
- B.H. Wouters, T. Chen, P.J. Grobet, *J. Phys. Chem. B* 105 (2001) 1135–1139.

- [34] T.H. Chen, B.H. Wouters, P.J. Grobet, *Eur. J. Inorg. Chem.* (2000) 281–285.
- [35] M.J. Remy, D. Stanica, G. Poncelet, E.J.P. Feijen, P.J. Grobet, J.A. Martens, P.A. Jacobs, *J. Phys. Chem.* 100 (1996) 12440–12447.
- [36] T.H. Chen, B. Wouters, P. Grobet, *Chemical J. Internet* 2 (2000) 7–13.
- [37] J. Chen, T. Chen, N. Guan, J. Wang, *Catal. Today* 93–95 (2004) 627–630.
- [38] M.-C. Silaghi, C. Chizallet, J. Sauer, P. Raybaud, *J. Catal.* 339 (2016) 242–255.
- [39] F. Wakabayashi, J. Kondo, A. Wada, K. Domen, C. Hirose, *J. Phys. Chem.* 97 (1993) 10761–10768.
- [40] V.L. Zholobenko, M.A. Makarova, J. Dwyer, *J. Phys. Chem.* 97 (1993) 5962–5964.
- [41] W.M. Meier, *Zeitschrift für Kristallographie - New. Cryst. Struct.* 115 (1961) 439–450.
- [42] S. Yang, C. Yu, L. Yu, S. Miao, M. Zou, C. Jin, D. Zhang, L. Xu, S. Huang, *Angew. Chem. Int. Ed.* 56 (2017) 12553–12556.
- [43] A. Van De Runstraat, J.A. Kamp, P.J. Stobbelaar, J. Van Grondelle, S. Krijnen, R.A. Van Santen, *J. Catal.* 171 (1997) 77–84.
- [44] F. Ribeiro, C. Marcilly, M. Guisnet, *J. Catal.* 78 (1982) 267–274.
- [45] A.Y. Stakheev, E.S. Shpiro, O.P. Tkachenko, N.I. Jaeger, G. Schulz-Ekloff, *J. Catal.* 169 (1997) 382–388.
- [46] P. Kubanek, H.W. Schmidt, B. Spliethoff, F. Schüth, *Microporous Mesoporous Mater.* 77 (2005) 89–96.
- [47] O. Bortnovsky, P. Sazama, B. Wichterlova, *Appl. Catal. A* 287 (2005) 203–213.
- [48] A. Corma, J. Planelles, J. Sánchez-Marín, F. Tomás, *J. Catal.* 93 (1985) 30–37.
- [49] H. Matsuura, N. Katada, M. Niwa, *Microporous Mesoporous Mater.* 66 (2003) 283–296.
- [50] S. Schallmoser, T. Ikuno, M.F. Wagenhofer, R. Kolvenbach, G.L. Haller, M. Sanchez-Sanchez, J.A. Lercher, *J. Catal.* 316 (2014) 93–102.
- [51] A. Corma, A. Martínez, P.A. Arroyo, J.L.F. Monteiro, E.F. Sousa-Aguiar, *Appl. Catal. A* 142 (1996) 139–150.
- [52] S. Li, A. Zheng, Y. Su, H. Zhang, L. Chen, J. Yang, C. Ye, F. Deng, *J. Am. Chem. Soc.* 129 (2007) 11161–11171.
- [53] C. Song, Y. Chu, M. Wang, H. Shi, L. Zhao, X. Guo, W. Yang, J. Shen, N. Xue, L. Peng, W. Ding, *J. Catal.* 349 (2017) 163–174.
- [54] C. Song, M. Wang, L. Zhao, N. Xue, L. Peng, X. Guo, W. Ding, W. Yang, Z. Xie, *Chin. J. Catal.* 34 (2013) 2153–2159.